JACS
JOURNAL OF THE AMERICAN CHEMICAL SOCIETY
Article
pubs.acs.org/JACS

Band Structure Engineering by Substitutional Doping in Solid-State Solutions of [5-Me-PLY(O,O)]$_2$B$_{(1-x)}$Be$_x$ Radical Crystals

Pradip Bag, Mikhail E. Itkis, Dejan Stekovic, Sushanta K. Pal, Fook S. Tham, and Robert C. Haddon*

Department of Chemistry and Chemical & Environmental Engineering, University of California, Riverside, California 92521, United States

Supporting Information

ABSTRACT: We report the substitutional doping of solid-state spiro-bis(5-methyl-1,9-oxido-phenalenyl)boron radical ([**2**]$_2$B) by co-crystallization of this radical with the corresponding spiro-bis(5-methyl-1,9-oxido-phenalenyl)beryllium compound ([**2**]$_2$Be). The pure compounds crystallize in different space groups ([**2**]$_2$B, $P\bar{1}$, Z = 2; [**2**]$_2$Be, $P2_1/c$, Z = 4) with distinct packing arrangements, yet we are able to isolate crystals of composition [**2**]$_2$B$_{(1-x)}$Be$_x$, where x = 0−0.59. The phase transition from the $P\bar{1}$ to the $P2_1/c$ space group occurs at x = 0.1, but the conductivities of the solid solutions are enhanced and the activation energies reduced for values of x = 0−0.25. The molecular packing is driven by the relative concentration of the spin-bearing ([**2**]$_2$B) and spin-free ([**2**]$_2$Be) molecules in the crystals, and the extended Hückel theory band structures show that the progressive incorporation of spin-free [**2**]$_2$Be in the lattice of the [**2**]$_2$B radical (overall bandwidth, W = 1.4 eV, in the pure compound) leads to very strong narrowing of the bandwidth, which reaches a minimum at [**2**]$_2$Be (W = 0.3 eV). The results provide a graphic picture of the structural transformations undergone by the lattice, and at certain compositions we are able to identify distinct structures for the [**2**]$_2$B and [**2**]$_2$Be molecules in a single crystalline phase.

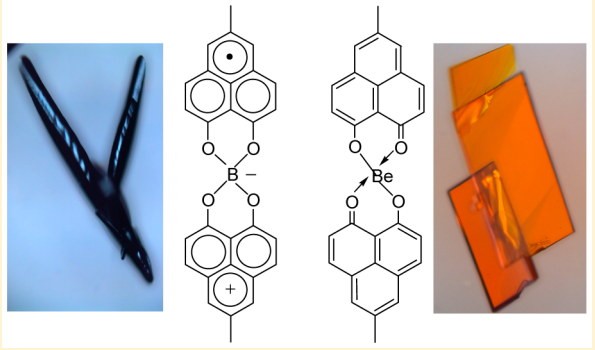

INTRODUCTION

New developments in the area of single-component organic conductors have led to the characterization of molecular metals[1−4] and superconductors[5] often as a result of the application of pressure.[6] An additional opportunity afforded by the single-component conductors is the possibility of realizing substitutionally doped materials in analogy with the classical semiconductors such as silicon where the carrier concentration is adjusted by the substitution of silicon atoms with boron (to introduce holes) or nitrogen (to introduce electrons) by making use of dopant atoms from adjacent columns of the periodic table. While the important role played by the substitutional doping of semiconductors such as silicon is well recognized, analogous studies based on purely organic molecular conductors are limited,[7−10] and it had not been previously possible to realize the molecular analogue of the atomic doping of silicon before we achieved the substitutional doping of the spiro-bis(1,9-oxido-phenalenyl)boron radical ([**1**]$_2$B) by doping with the analogous spiro-bis(phenalenyl) beryllium compound (Scheme 1, [**1**]$_2$Be).[11]

In our experiments the dopant molecules, [**1**]$_2$Be, are neutral, and they furnish holes in the crystalline lattice of [**1**]$_2$B radicals. We were previously able to prepare a range of substitutionally doped compounds of composition [**1**]$_2$B$_{(1-x)}$Be$_x$ (where x = 0−0.2), and we found that many of the solid-state mixtures showed an increase in conductivity and a decrease in the activation energy (Δ) for the conduction process—the maximum conductivity was attained at x = 0.07 (σ_{RT} > 1 S/cm, Δ = 0.05 eV), which represents an order of magnitude increase in the conductivity of the parent system ([**1**]$_2$B).[12] These results suggest that the substitutional doping of organic molecular crystals is a promising new direction in organic solid-state chemistry, and in the present article we report the crystallization of a second substitutionally doped organic material [**2**]$_2$B$_{(1-x)}$Be$_x$ based on the host radical [**2**]$_2$B ([5-Me-PLY(O,O)]$_2$B) (Scheme 1).[12] [See nomenclature definition in refs 13 and 14.] We show that co-crystallization of the [**2**]$_2$B radical with the analogous [**2**]$_2$Be compound also leads to enhanced conductivities, and in the present case we are able to co-crystallize a much greater range of stoichiometries which encompass structures characteristic of both pure phases; thus, we find space groups $P\bar{1}$ (triclinic, Z = 2, for x = 0−0.1) and $P2_1/c$ (monoclinic, Z = 4, for x = 0.1−1), both of which show increased conductivities relative to those of the parent compounds. Within the $P2_1/c$ space group, however, the band structures are a strong function of composition, and for stoichiometries of x = 0.13, 0.26, and 0.59 we are able to separately refine the [**2**]$_2$B and [**2**]$_2$Be crystallographic lattices, which show distinct electronic structures.

Received: June 12, 2015
Published: August 3, 2015

DOI: 10.1021/jacs.5b06145
J. Am. Chem. Soc. 2015, 137, 10000−10008

Scheme 1. Synthesis of $[2]_2B_{(1-x)}Be_x$ Crystals by Chemical Reduction

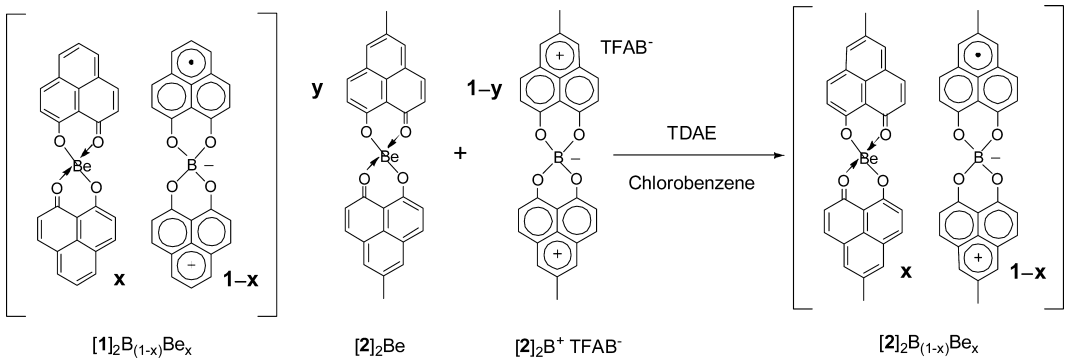

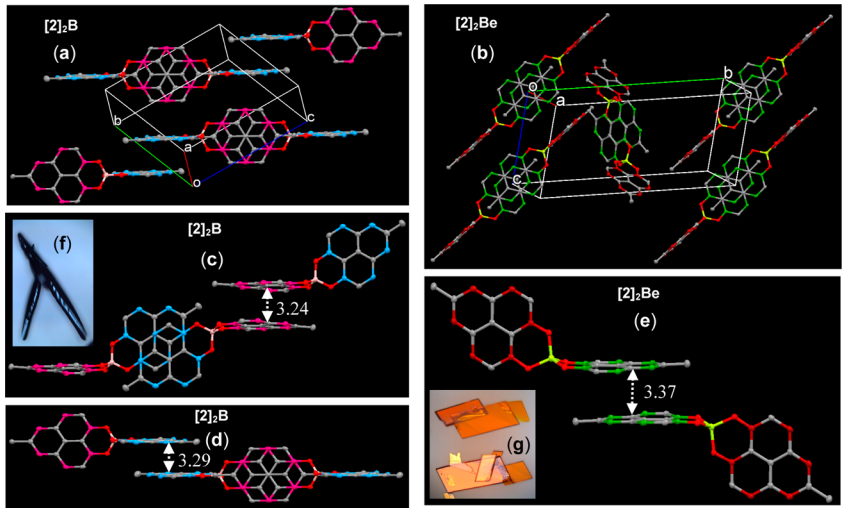

Figure 1. Single-crystal X-ray structures of $[2]_2B$ (space group $P\bar{1}$, $Z = 2$) and $[2]_2Be$ ($P2_1/c$, $Z = 4$): (a) 1D π-chains of $[2]_2B$, (b) dimers of $[2]_2Be$, (c–e) interplanar $\pi-\pi$ separations, and (f,g) pictures of crystals.

Scheme 2. (a) Phenalenyl Structure[a] and (b–d) Bernal Stacked Graphene Fragments Showing Stacking Motifs Observed in the Phenalenyl Units of $[1]_2B$, $[1]_2Be$, $[2]_2B$, and $[2]_2Be$[b]

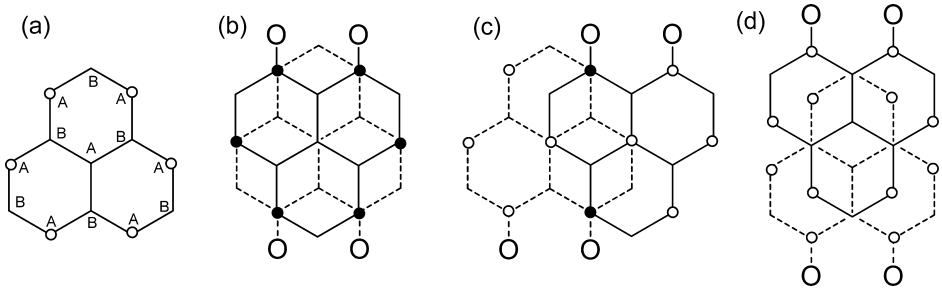

[a]Chosen labels for the two sub-lattices (A, B) are shown, together with the sites of non-vanishing spin density in the non-bonding molecular orbital (NBMO, SOMO); ○ = active positions. [b]Sub-lattice and formal site of SOMO spin density in radicals: ● = active positions, superimposed; ○ = active positions, non-superimposed; no symbol = B sub-lattice and formal site of SOMO node in radical, inactive position; O = oxygen substituents. (b) π-stacking in $[1]_2B$, $[1]_2Be$, and $[2]_2B$ (one PLY unit); (c) π-stacking in $[2]_2B$ (one PLY unit); and (d) π-stacking in $[2]_2Be$.

RESULTS AND DISCUSSION

Synthesis. Substitutionally doped crystals of composition $[2]_2B_{(1-x)}Be_x$ were prepared from solutions of $[2]_2B^+TFAB^-$ ($TFAB^-$ = tetrakis(pentafluorophenyl)borate) and $[2]_2Be$ in chlorobenzene by reduction with tetrakis(dimethylamino)-ethylene (TDAE) by direct mixing inside an inert atmosphere glovebox. The electrochemistry of the two precursors is similar to that of the $[1]_2B$, $[1]_2Be$ pair, with reduction potentials $E_{1/2}$ = −0.36, −0.64 V ($[2]_2B^+TFAB^-$) and $E_{1/2}$ = −1.40, −1.69 V ($[2]_2Be$) (Supporting Information). Thus, $[2]_2Be$ is much more difficult to reduce than $[2]_2B^+TFAB^-$, and hence the crystallization process is driven by the insolubility of radical $[2]_2B$, which apparently induces the co-crystallization of $[2]_2Be$. There is extensive evidence to support the strong π-association of pairs of PLY units which together possess one or two spins,[15−19] and this interaction is apparently sufficient to ensure an appreciable concentration of $[2]_2Be$ in the final structures: thus we were able to prepare a series of mixed

DOI: 10.1021/jacs.5b06145
J. Am. Chem. Soc. 2015, 137, 10000−10008

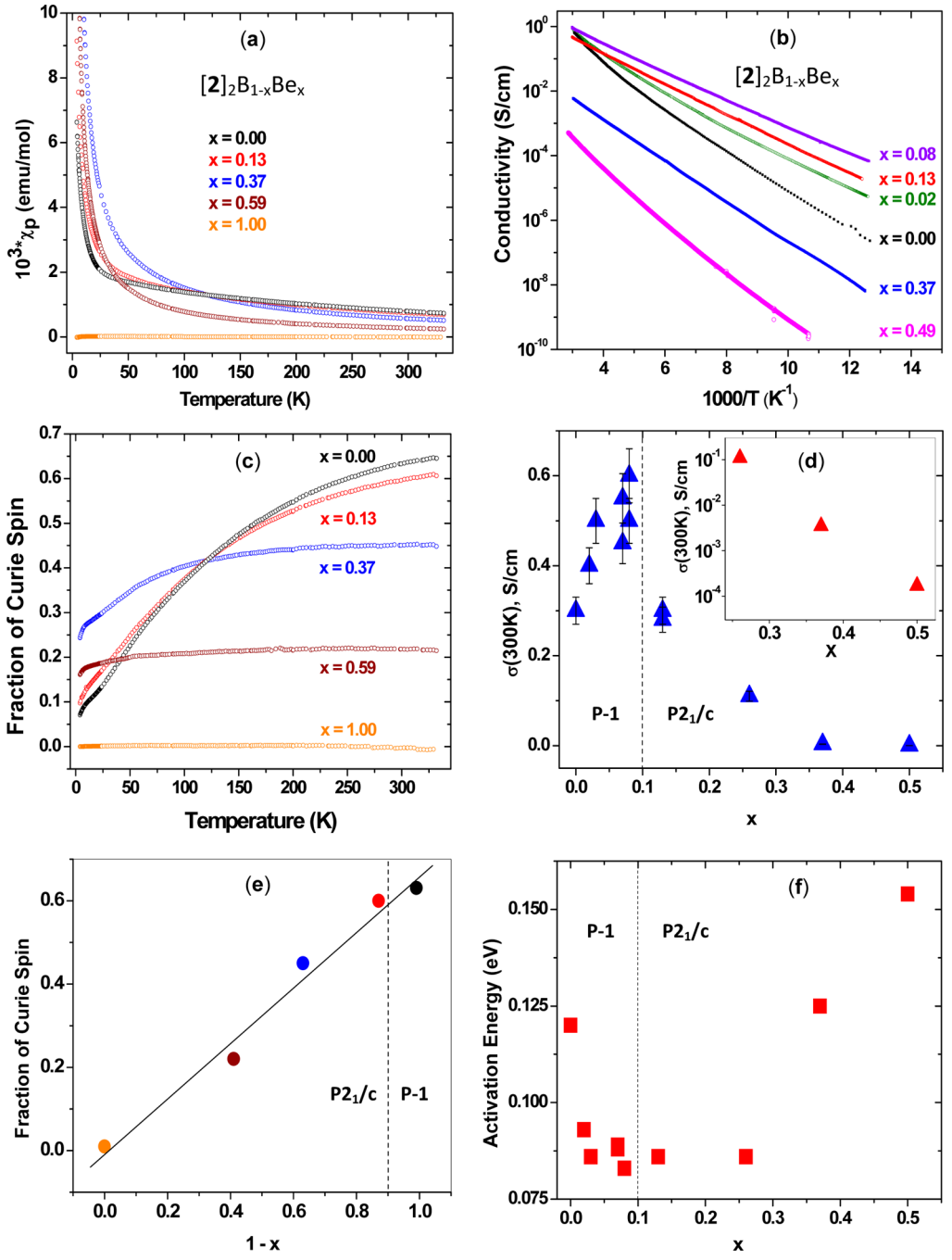

Figure 2. Electrical and magnetic properties of $[2]_2B$, $[2]_2Be$, and $[2]_2B_{(1-x)}Be_x$. (a) Magnetic susceptibility of $[2]_2B_{(1-x)}Be_x$ (x = 0, 0.13, 0.37, 0.59, and 1). (b) Single-crystal conductivity of $[2]_2B_{(1-x)}Be_x$ as a function of reciprocal temperature. (c) Fraction of Curie spins as a function of temperature. (d) Room-temperature conductivity as a function of x (inset shows the same data on a logarithmic scale). (e) Fraction of Curie spins as a function of the concentration of radicals in the lattice ($1 - x$) in the high temperature limit (T = 300 K). (f) Activation energy as a function of the concentration of $[2]_2Be$ (x).

$[2]_2B_{(1-x)}Be_x$ crystals of composition $0 > x > 0.59$, as determined by direct ICP chemical analysis of the amount of beryllium in the samples together with the pure phases, x = 0 and 1.

Structure. While the neutral radical $[2]_2B$ co-crystallizes with $[2]_2Be$ to form a series of solid-state mixtures $[2]_2B_{(1-x)}Be_x$, the molecular packing in the crystal structure of the pure beryllium compound is quite different from that observed in the parent spiro-bis(phenalenyl)boron radical, $[2]_2B$.[12] The crystal structure of the parent radical is triclinic (space group $P\bar{1}$, Z = 2, Figure 1a,c,d), and consists of infinite π-chains, whereas the pure beryllium compound crystallizes in a monoclinic unit cell (space group $P2_1/c$, Z = 4, Figure 1b,e) and exhibits a dimeric packing arrangement. Solid-state solutions of $[2]_2B_{(1-x)}Be_x$ crystallize as both the triclinic and monoclinic phases depending on the fraction of $[2]_2Be$ molecules in the lattice: at low concentrations ($x < 0.1$) the doped crystals adopt triclinic structures whereas at higher concentrations (x = 0.1–0.59, 1), monoclinic phases prevail (the crystal chemistry of the compounds is discussed in more

DOI: 10.1021/jacs.5b06145
J. Am. Chem. Soc. 2015, 137, 10000–10008

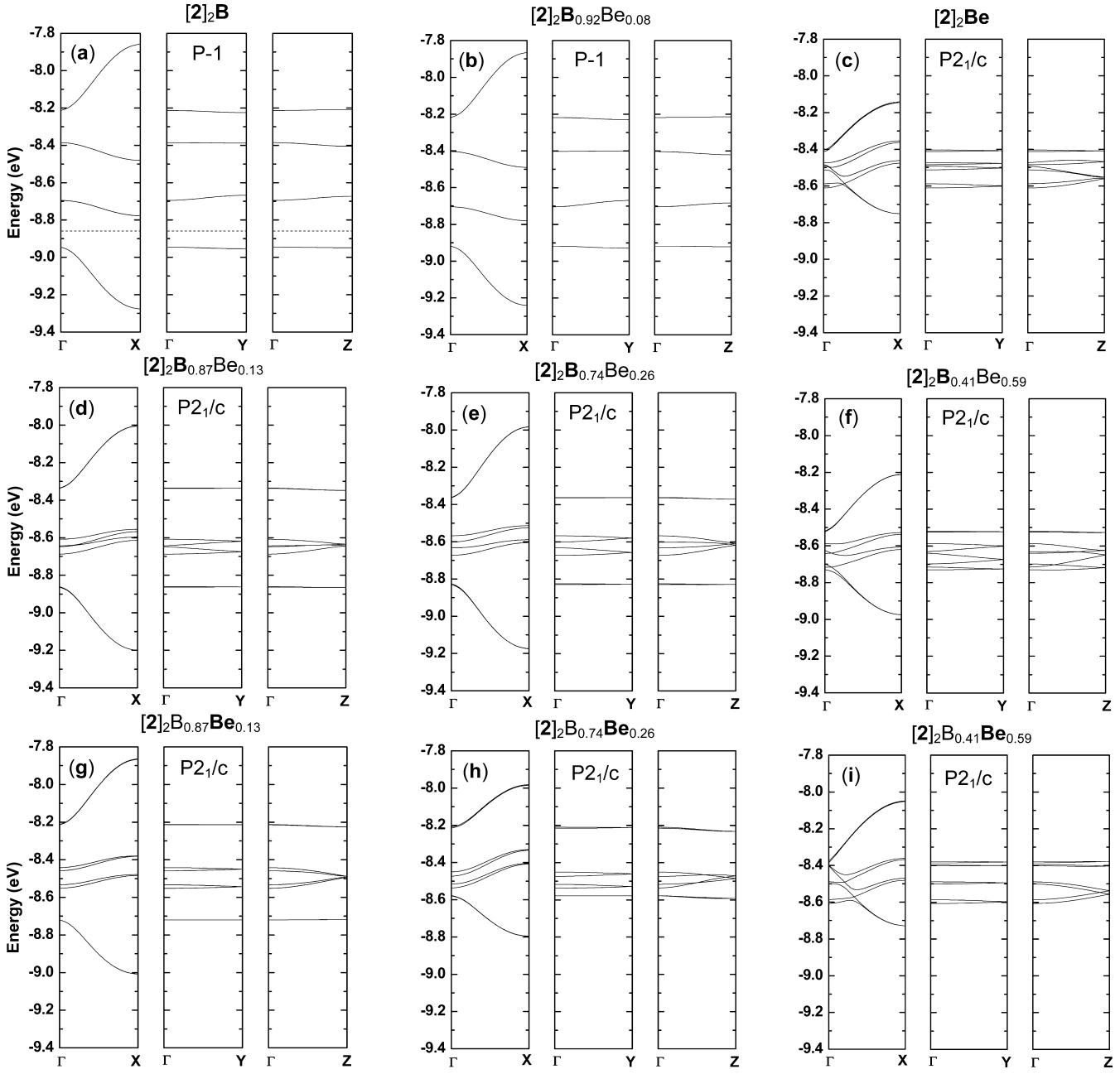

Figure 3. Extended Hückel theory band structures calculated for the experimental structures of crystalline $[\mathbf{2}]_2B_{(1-x)}Be_x$ as a function of x (see text and Methods section). In all cases the calculations are based on a single lattice which contains either $[\mathbf{2}]_2B$ or $[\mathbf{2}]_2Be$ molecules, and in the solid solutions the chosen lattice is shown in bold type in the formula. (d–i) X-ray refinement led to the identification of both the $[\mathbf{2}]_2B$ and $[\mathbf{2}]_2Be$ molecules in the structures where x = 0.13, 0.26, and 0.59, and in those cases the band structures of both lattices are shown. Thus, (d) and (g) refer to the $[\mathbf{2}]_2B$ and $[\mathbf{2}]_2Be$ lattices, respectively, in the $[\mathbf{2}]_2B_{0.74}Be_{0.26}$ crystal. The Fermi level of (a) is shown in the panel, and with the exception of (c), the Fermi level lies in the lowest band of the $P\bar{1}$ point group compositions and in the lowest two bands of the $P2_1/c$ point group compositions of the $[\mathbf{2}]_2B$ lattice.

detail in conjunction with the band structure calculations). The structural behavior of the new compounds are therefore quite distinct from that of $[\mathbf{1}]_2B_{(1-x)}Be_x$ in which the pure phases and all intermediate compositions crystallize as π-chains in a monoclinic space group ($C2/c$), and mixed crystals are only isolable in the range x = 0.0–0.2.

In the original synthesis of $[\mathbf{2}]_2B$[12] it was found that the presence of a methyl group at the 5-position prevents the perfect superposition of the PLY units that is characteristic of $[\mathbf{1}]_2B$.[12] This results in a π-chain structure in which one PLY subunit is fully superimposed on a neighboring PLY unit with a bend at the oxygen atom (Scheme 2a,b), while the other PLY subunit adopts a slipped π-overlap structure (Scheme 2c). Thus, $[\mathbf{2}]_2B$ has two different PLY–PLY interactions along the π-chains, one in which there is superposition of the seven spin bearing carbons while the other contains only three overlapped spin bearing carbons (Scheme 2a–c) This creates a bowing effect on the superimposed PLYs such that the central carbons approach more closely (3.14 Å C···C separation) than the carbons at the ends of the molecules leading to a mean plane separation of 3.24 Å for the fully superimposed PLY units. In the case of the slipped, partial π-overlap between PLY units in

DOI: 10.1021/jacs.5b06145
J. Am. Chem. Soc. 2015, 137, 10000–10008

$[\mathbf{2}]_2$B, there is registry between each of the central carbons and three of the fully spin-bearing carbon atoms, and the mean plane separation is 3.29 Å (Scheme 2c).[12]

It has been pointed out that the phenalenyl radical can be viewed as a molecular building block of graphene.[20,21] It is also useful to consider the 3-D solid-state stacking of the spiro-bis(phenalenyl) compounds $[\mathbf{1}]_2$B, $[\mathbf{1}]_2$Be, $[\mathbf{2}]_2$B, and $[\mathbf{2}]_2$Be from the standpoint of the stacked version of graphene—that is, graphite. In graphene there are two sub-lattices (usually labeled A and B), which contain carbon atoms that are chemically equivalent but crystallographically distinct. In the Bernal structure of graphite the symmetry between the two sub-lattices is lifted because one sub-lattice of atoms lies directly over the atoms in a neighboring plane, while the other sub-lattice atoms lie over the centers of the benzene rings in the adjacent plane (Scheme 2). In the case of the phenalenyl molecule, the symmetry is lifted by the finite size of the molecules, and the odd number of carbon atoms differentiates the sub-lattices; we label the sub-lattice possessing an extra carbon atom as A, and it is this sub-lattice which will bear the spin density (active positions) in the radical form (Scheme 2a).[20,21] Thus, the most prevalent form of π-association involves stacking of the PLY units so that the radical spin-bearing atoms (sub-lattice A of both molecules) are in full registry, thereby ensuring strong SOMO–SOMO orbital overlap (pancake bonding, Scheme 2b),[5,15−19,22−26] and this is what is observed in the case of $[\mathbf{1}]_2$B (both ends of the molecule) and $[\mathbf{2}]_2$B (one end of the molecule); the other end of $[\mathbf{2}]_2$B stacks with partial π-overlap of the active carbon atoms (Scheme 2c).

The packing of the beryllium compounds is quite unusual in that $[\mathbf{1}]_2$Be (π-chain) adopts exactly the same mode of π-stacking as in $[\mathbf{1}]_2$B (Scheme 2b), even though the PLY units of the beryllium compound do not contain unpaired electrons. The solid-state structure of $[\mathbf{2}]_2$Be (π-dimer) also involves sub-lattice registry, but this time four atoms of the B sub-lattices of both molecules are involved (Scheme 2d). In the case of $[\mathbf{1}]_2$Be and $[\mathbf{2}]_2$Be, the interplanar separations are 3.40 and 3.37 Å, which are considerably longer than the π-stacking involving spin-bearing PLY units but nevertheless suggests that van der Waals dispersion forces are sufficient to maintain π-stacked structures in the absence of pancake bonding.[18,19,26]

Physical Measurements. The magnetic susceptibility and electrical conductivity data for compounds $[\mathbf{2}]_2$B, $[\mathbf{2}]_2$Be, and $[\mathbf{2}]_2\mathrm{B}_{(1-x)}\mathrm{Be}_x$ are summarized in Figure 2, and it is clear that the replacement of $[\mathbf{2}]_2$B radicals by $[\mathbf{2}]_2$Be molecule in the lattice has two main effects on the magnetism of the crystals. The substitution of diamagnetic $[\mathbf{2}]_2$Be for paramagnetic $[\mathbf{2}]_2$B decreases the paramagnetic susceptibility of the crystals in the high temperature limit, and this is apparent in the linear relationship between the fraction of Curie spins and the composition of the crystals. The second effect is reflected in the reduced temperature dependence of the fraction of Curie spins as the concentration of $[\mathbf{2}]_2$Be is increased. This is best explained by the resonating valence bond (RVB) ground state suggested for the parent system $[\mathbf{2}]_2$B,[11,12,27] in which the majority of spins are coupled in antiferromagnetic RVB pairs.[28,29] Inserting diamagnetic PLY units into the lattice leaves isolated PLY radicals which behave as paramagnetic (Curie) spins. This is especially evident in $[\mathbf{2}]_2\mathrm{B}_{0.41}\mathrm{Be}_{0.59}$ where the fraction of Curie spins as a function of temperature is almost independent of temperature (Figure 2c). The conductivity of the crystals increases with doping until the $P\bar{1}$ lattice become unstable (x = 0.1), and attains its highest value at a composition of 8% beryllium ($[\mathbf{2}]_2\mathrm{B}_{0.92}\mathrm{Be}_{0.08}$), where it reaches σ_{RT} = 0.6 S/cm (twice that of the parent radical, $[\mathbf{2}]_2$B), just before the space group changes to $P2_1/c$. The activation energy also falls in this range of compositions but stays at relatively low values through the phase transition until a composition of x = 0.26 is reached (Figure 2f). The smooth evolution of the magnetic and conductivity properties of $[\mathbf{2}]_2\mathrm{B}_{(1-x)}\mathrm{Be}_x$ through the phase transition at x = 0.1 seems quite surprising, but the band structure calculations reflect the regular progression in the band dispersions in k-space (apart from the doubling of the unit cell along the b-axis as the space group changes from triclinic to monoclinic).

Electronic Band Structure and Crystal Packing. Figure 3 shows the band structures arising from the PLY SOMOs in the $[\mathbf{2}]_2\mathrm{B}_{(1-x)}\mathrm{Be}_x$ solid solutions, and there is relatively strong dispersion along the x-axes at all compositions; the dispersion of the lowest band of $[\mathbf{2}]_2$B (0.40 eV) is slightly higher than the other compositions which reach a value of about 0.35 eV in the range x = 0.03–0.25, in agreement with the minima found in the experimental activation energies of the conductivities. The bandwidth of the complex (W) attains its maximum value at $[\mathbf{2}]_2$B and decreases monotonically as x increases in the $[\mathbf{2}]_2\mathrm{B}_{(1-x)}\mathrm{Be}_x$ compositions (Figure 4d). As noted previously, the regular evolution of the band structures with composition is the most notable feature of these results. It may be seen in the band structures at low doping levels (x = 0–0.1) that $[\mathbf{2}]_2$B dominates the electronic structure and a rigid band approximation is adequate.

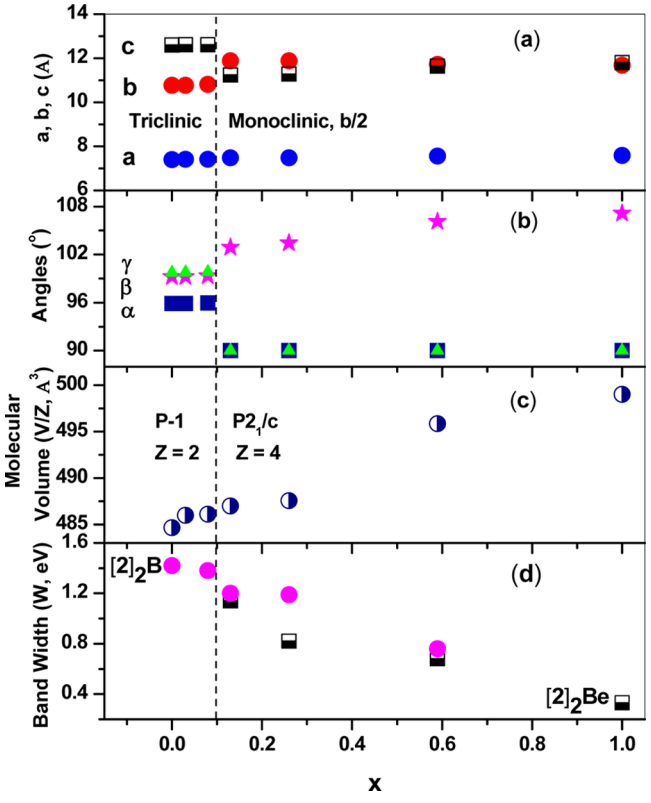

Figure 4. (a,b) Unit cell parameters of $[\mathbf{2}]_2\mathrm{B}_{(1-x)}\mathrm{Be}_x$ (x = 0–1) as a function of composition. (c) Molecular volume, where V (Å^3) is the unit cell volume and Z is the number of molecules in the unit cell. (d) Bandwidth (W, eV).

DOI: 10.1021/jacs.5b06145
J. Am. Chem. Soc. 2015, 137, 10000–10008

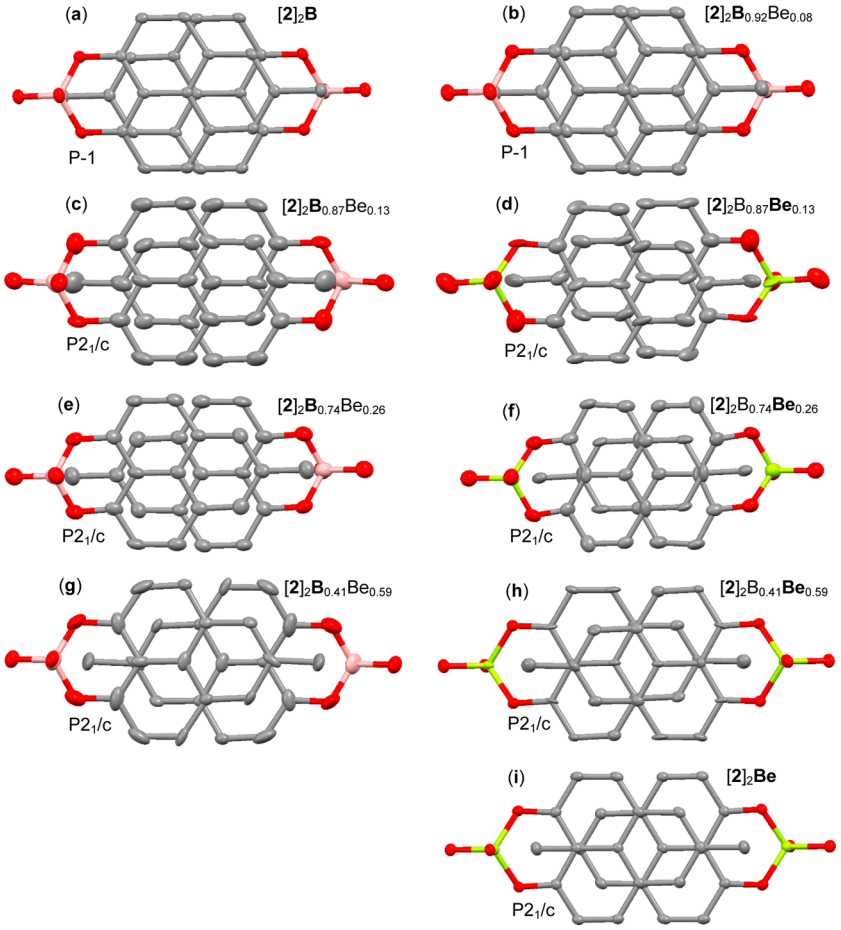

Figure 5. Perpendicular view of the π-stacked PLY rings which undergo slippage in the $P2_1/c$ phase as a function of composition. As the concentration of $[\mathbf{2}]_2$Be molecules increases in the lattice, the dimer pair present in $[\mathbf{2}]_2$B (Scheme 2b) is transformed into the dimer pair present in the $[\mathbf{2}]_2$Be crystals (Scheme 2d), and thus the fully registered π-stacking present in $[\mathbf{2}]_2$B eventually adopts the $[\mathbf{2}]_2$Be structure in which all π-bonding between PLY units is removed.

At compositions where $x > 0.1$, the presence of $[\mathbf{2}]_2$Be in the lattice exerts a number of important effects. First the unit cell doubles in size and changes in symmetry ($P\bar{1}$ to $P2_1/c$), as molecules of $[\mathbf{2}]_2$Be are incorporated in the lattice—as we noted previously the presence of molecular spins dictates specific intermolecular interactions which are not favorable in the case of spin-free molecules such as of $[\mathbf{2}]_2$Be,[11] and the transition to the $P2_1/c$ structure is accompanied by the complete loss of the slipped π-stacking along the π-chain (Figure 1c, Scheme 2c). The localization of the electronic structure in the $P2_1/c$ structure is strongly reflected in the band structure calculations where it may be seen that the bandwidth narrows with increasing values of x as intermolecular interactions become less important throughout the crystals. A particularly dramatic manifestation of this competition between the very different packing requirements of $[\mathbf{2}]_2$B and $[\mathbf{2}]_2$Be molecules is the emergence of two lattices, which were separately refined in the crystal structure determination for three compositions of the $[\mathbf{2}]_2\mathrm{B}_{(1-x)}\mathrm{Be}_x$ crystals (x = 0.13, 0.26, 0.59). There are strong distinctions in the band structures of the $[\mathbf{2}]_2$B and $[\mathbf{2}]_2$Be lattices at these compositions, with smaller bandwidths (W) for the $[\mathbf{2}]_2$Be lattice, and the divergence between the two lattice structures reaches a maximum at x = 0.26, where W = 1.19 eV ($[\mathbf{2}]_2$B) and 0.82 eV ($[\mathbf{2}]_2$Be)(Figure 4d).

The transition from $P\bar{1}$ to $P2_1/c$ space groups occurs at about x = 0.1, but it is important to note that total width of the band complex is largely maintained through this phase transition; for example W = 1.2 eV in $[\mathbf{2}]_2\mathrm{B}_{0.87}\mathrm{Be}_{0.13}$ even though the slipped π-stacking (Figure 1c, Scheme 2c) is completely lost in the $P2_1/c$ structure. Closer inspection of the band structures shows that the strong dispersion along the a-direction for $x \approx 0$–0.5 arises from the fully superimposed π-overlap (Figure 1a, Scheme 2b), which actually transforms into the π-overlap of nonactive carbon atoms which occurs in $[\mathbf{2}]_2$Be (Figure 1b, Scheme 2d) by slippage of pairs of PLY molecules with respect to each other, and it is this translation across the molecular surfaces which serves to turn off the conducting pathway (quite apart from the drop in the carrier concentration). The two molecular lattices translate at different rates with respect to the change in composition, and the $[\mathbf{2}]_2$Be molecules move much more readily than the $[\mathbf{2}]_2$B molecules (most apparent in the $[\mathbf{2}]_2\mathrm{B}_{0.74}\mathrm{Be}_{0.26}$ structure, Figure 5e,f). The important conclusion from the foregoing analysis is the recognition that in substitutionally doped organic semiconductors, the conductivity is not just a function of band filling within a rigid band model, but that the lattice responds to accommodate the presence of spin-bearing and spin-free molecules because the packing is not determined by fully developed covalent bonds.

DOI: 10.1021/jacs.5b06145
J. Am. Chem. Soc. 2015, 137, 10000–10008

CONCLUDING REMARKS

While we have noted the strong distinctions between the detailed electronic structures of $[\mathbf{1}]_2B_{(1-x)}Be_x$[11] and $[\mathbf{2}]_2B_{(1-x)}Be_x$, the gross features of the phase diagrams share some similarities. At low doping levels ($x \leq 0.15$), substitutional doping is effective and increases the conductivity while lowering the activation energy of both compounds. However, beyond this point it becomes very difficult to prepare solid solutions in the case of $[\mathbf{1}]_2B_{(1-x)}Be_x$,[11] because the lattice parameters suffer such drastic changes in passing from the $[\mathbf{1}]_2B$ to the $[\mathbf{1}]_2Be$ unit cell, even though the space group and mode of packing remain unchanged throughout. In the case of $[\mathbf{2}]_2B_{(1-x)}Be_x$, apart from a doubling of the unit cell size, the lattice constants are largely maintained (Figure 4) while accommodating drastic changes in the mode of packing which lead to extreme band narrowing (Figures 3 and 4). In short, both compounds show a substiutional doping regime for values of $x \leq 0.15$ but rather different behaviors when the rigid band model starts to fail.

While the spin of the electron has become recognized as an important tool in a number of distinct avenues including functional materials,[30−38] electrocatalysis,[39] spintronics,[40−42] and quantum computing,[43] its importance in the structural control of the packing in molecular solids is not well known. While it may be difficult to anticipate the effects of spin on molecular structure, it is clear that these interactions can play a very important role in determining the crystal structure, and in crystals involving mixtures of radicals and spin-free molecules of similar size and electronic structure (as discussed herein), there is a clear competition between the structural preferences of the constituent molecules. The introduction of spin-free molecules into a lattice of radicals may be viewed as having the opposite effect of physical pressure in that the lattice expands due to the reduction in strength of the intermolecular bonding, and this is apparent from the bandwidths and unit cell volumes of both $[\mathbf{1}]_2B_{(1-x)}Be_x$[11] and $[\mathbf{2}]_2B_{(1-x)}Be_x$ (Figures 4 and 5).

We note again that the increase in conductivity of the doped crystals is unexpected when viewed from the standpoint of substitutionally doped semiconductors,[11] because the electrochemistry suggests that the dopant energy levels which originate from $[\mathbf{2}]_2Be$ will lie much too high in energy to contribute to the transport properties of the doped $[\mathbf{2}]_2B_{(1-x)}Be_x$ crystals. However, if viewed from the RVB standpoint, the increase in conductivity would be expected as doping will disrupt the antiferromagnetic RVB pairs resulting in increased conductivity.[28,29,44] While the doped semiconductor analogy motivated our original work, it is clear from the compounds isolated to date that there are limitations in extrapolating this model to organic molecular solids.[11] First and foremost is the issue of the energy levels at low doping levels (above), but the strong evolution of the dispersion in the band structures of the doped $[\mathbf{2}]_2B_{(1-x)}Be_x$ crystals when $x > 0.1$ (Figure 3) emphasizes the failure of the rigid band model, which is known to be quite effective for classical semiconductors[45] and even the doped C_{60} phases.[46]

EXPERIMENTAL AND CALCULATIONAL METHODS

Materials. All reactions and manipulations were carried out under an atmosphere of dry argon using standard Schlenk and vacuum-line techniques. The reagents 1.0 M BCl_3 solution in hexane (Aldrich), $Be(acac)_2$ (Aldrich), tetrakis(dimethylamino)ethylene (TDAE, TCI America), and potassium tetrakis(pentafluorophenyl)borate (K^+TFAB^-, Boulder Scientific Company) were used as received. $[\mathbf{2}]_2B^+TFAB^-$ was synthesized according to literature procedures, and $[\mathbf{2}]_2Be$ was synthesized by a modification of the original procedure.[12,47,48]

Dry acetonitrile and chlorobenzene were purchased from Aldrich. Cyclic voltammetric measurement were performed on a CH instrument using a Pt disk electrode in dry acetonitrile under argon atmosphere with n-Bu_4NPF_6 as the supporting electrolyte with a standard calomel reference electrode, and the ferrocenium/ferrocene couple was used as internal reference. ESI mass spectra were recorded with a Agilent LCTOF (2006), machine with APCI/ESI ionization. MALDI mass spectra were obtained on a Voyager-DE STR BioSpectrometry Workstation mass spectrometer. NMR spectra were recorded on a Bruker 300 spectrometer. Elemental analyses and inductively coupled (ICP) mass spectrometry analyses of the $[\mathbf{2}]_2B_{1-x}Be_x$ samples (10 mg) were performed at the Microanalysis Laboratory, University of Illinois, Urbana−Champaign, IL.

Synthesis of $[\mathbf{2}]_2Be$. Beryllium acetylacetonate (1 mmol, 0.207 g) was added to a stirred THF (20 mL) solution of 5-methyl-9-hydroxyphenalenone (2 mmol, 0.42 g)[49] in an argon atmosphere, and the mixture was stirred at 60 °C for 2 days. The yellow solid which deposited was filtered and washed with ether. Yield 0.32 g (75%); mp > 350 °C; ^1H NMR (300 MHz, $CDCl_3$, 25 °C) δ 8.13 (2H, d), 7.90 (dH, s), 7.24 (2H, d), 2.64 (3H, s) ppm; ESI-MS m/z calcd for $C_{28}H_{19}O_4Be$ [MH^+], 428.1405, found 428.1425. Anal. Calcd (found) for $C_{28}H_{18}O_4Be$: C, 78.68 (78.55); H, 4.24 (4.30).

General Method of Synthesis and Crystallization of Doped Radicals $[\mathbf{2}]_2B_{1-x}Be_x$. In a typical experiment (preparation of $[\mathbf{2}]_2B_{0.74}Be_{0.26}$) which was conducted in a glovebox, a solution of 13 mg (3.04×10^{-5} mol) of $[\mathbf{2}]_2Be$ in 10 mL of dry chlorobenzene was transferred to a vial containing 33.7 mg (3.04×10^{-5} mol) of $[\mathbf{2}]_2B^+TFAB^-$. To this homogeneous solution, a drop of TDAE was added, and the vial was left undisturbed overnight. The black shining needle-shaped crystals (11 mg, yield 42%) which deposited on the walls of the vial were collected by filtration and washed with acetonitrile. The beryllium content ($x = 0.26$) was established by ICP analysis, and the compound was characterized by bulk magnetic susceptibility, single-crystal X-ray diffraction, and four-probe conductivity measurements. Crystals with other beryllium compositions ($x = 0.02$, 0.03, 0.08, 0.13, 0.26, 0.37, 0.49, and 0.59) were synthesized and crystallized by similar procedures.

X-ray Crystallography. Full details of the crystallography are included in the Supporting Information. A thin black plate-like fragment was used for the single-crystal X-ray diffraction study of $[\mathbf{2}]_2B_{0.74}Be_{0.26}$; the crystal was coated with paratone oil and mounted on a cryo-loop glass fiber. X-ray intensity data were collected at 100(2) K on a Bruker APEX2[50] platform CCD X-ray diffractometer system (fine-focus Mo radiation, $\lambda = 0.71073$ Å, 50 kV/35 mA power). The crystallographic parameters and unit cell dimensions are summarized in Table S1. Absorption corrections were applied to the raw intensity data using the SADABS program.[51] Atomic coordinates and isotropic and anisotropic displacement parameters of all the non-hydrogen atoms were refined by means of a full-matrix least-squares procedure on F^2. The H atoms were included in the refinement in calculated positions riding on the atoms to which they were attached.

Single-Crystal Near- and Mid-Infrared Transmission Spectroscopy. The infrared transmission measurements were carried out on single crystals using a FTIR Nicolet Nexus 670 ESP spectrometer integrated with a Thermo-Nicolet Continuum microscope.

Band Structure Calculation. The band structure calculations made use of a modified version of the extended Hückel theory band structure program supplied by M. H. Whangbo and were carried out according to methods detailed in previous reports.[52−55]

The calculations were carried out within a single unit cell, and thus all of the band structures refer to either the $[\mathbf{2}]_2B$ or $[\mathbf{2}]_2Be$ lattices for each composition. For certain compositions we were able to refine the structures of the two lattices independently, and in those cases the band structures of both the $[\mathbf{2}]_2B$ and the $[\mathbf{2}]_2Be$ molecules are given in Figure 3.

Conductivity Measurements. The single-crystal conductivities were measured in a four probe configuration using in line contacts which

DOI: 10.1021/jacs.5b06145
J. Am. Chem. Soc. 2015, 137, 10000−10008

were made with silver paint. The sample was placed on a sapphire substrate, and electrical connections between the silver paint contacts and substrate were made by thin flexible 25 μm diameter silver wire to relieve mechanical stress during thermal cycling of the sample. The conductivities were measured along the long axis of the crystals. The conductivity was measured in a custom-made helium variable-temperature probe using a Lake Shore 340 temperature controller in the range from 330 to 77 K. A Keithley 236 unit was used as a voltage source and current meter, and two 6517A Keithley electrometers were used to measure the voltage drop between the potential leads in a four probe configuration in which the instrumentation was driven with LabVIEW software.

Magnetic Susceptibility Measurements. The molar magnetic susceptibility of 10−15 mg samples of the crystalline powders were measured by utilizing a Vibrating Sample Magnetometer in an EverCool-II cryogen-free upgraded version of a Physical Property Measurement System (Quantum Design International, USA) in a magnetic field of 1 T over the temperature range from 330 to 4 K.

■ ASSOCIATED CONTENT

Supporting Information

The Supporting Information is available free of charge on the ACS Publications website at DOI: 10.1021/jacs.5b06145.

X-ray data for $[\mathbf{2}]_2B_{0.97}Be_{0.03}$ (CIF)
X-ray data for $[\mathbf{2}]_2B_{0.92}Be_{0.08}$ (CIF)
X-ray data for $[\mathbf{2}]_2B_{0.87}Be_{0.13}$ (CIF)
X-ray data for $[\mathbf{2}]_2B_{0.74}Be_{0.26}$ (CIF)
X-ray data for $[\mathbf{2}]_2B_{0.41}Be_{0.59}$ (CIF)
X-ray data for $[\mathbf{2}]_2Be$ (CIF)
Cyclic voltammetry, near- and mid-infrared transmission spectroscopy, and ICP and X-ray analysis, summarized in Table S1 (PDF)

■ AUTHOR INFORMATION

Corresponding Author

*haddon@ucr.edu

Notes

The authors declare no competing financial interest.

■ ACKNOWLEDGMENTS

This material is based upon work supported by the Division of Materials Science and Engineering, Office of Basic Energy Sciences, of the U.S. Department of Energy under Award No. DE-FG02-04ER46138.

■ REFERENCES

(1) Tanaka, H.; Okano, Y.; Kobayashi, H.; Suzuki, W.; Kobayashi, A. *Science* **2001**, *291*, 285.
(2) Tanaka, H.; Tokumoto, M.; Ishibashi, S.; Graf, D.; Choi, E. S.; Brooks, J. S.; Yasuzuka, S.; Okano, Y.; Kobayashi, H.; Kobayashi, A. *J. Am. Chem. Soc.* **2004**, *126*, 10518.
(3) Mailman, A.; Winter, S. M.; Yu, X.; Robertson, C. M.; Yong, W.; Tse, J. S.; Secco, R. A.; Liu, Z.; Dube, P. A.; Howard, J. A. K.; Oakley, R. T. *J. Am. Chem. Soc.* **2012**, *134*, 9886.
(4) Wong, J. W. L.; Mailman, A.; Lekin, K.; Winter, S. M.; Yong, W.; Zhao, J.; Garimella, S. V.; Tse, J. S.; Secco, R. A.; Desgreniers, S.; Ohishi, Y.; Borondics, F.; Oakley, R. T. *J. Am. Chem. Soc.* **2014**, *136*, 1070.
(5) Cui, H.; Kobayashi, H.; Ishibashi, S.; Sasa, M.; Iwase, F.; Kato, R.; Kobayashi, K. *J. Am. Chem. Soc.* **2014**, *136*, 7619.
(6) Haddon, R. C. *ChemPhysChem* **2012**, *13*, 3581.
(7) Porter, W. W., III; Vaid, T. P.; Rheingold, A. L. *J. Am. Chem. Soc.* **2005**, *127*, 16559.
(8) Porter, W. W., III; Vaid, T. P. *J. Mater. Chem.* **2007**, *17*, 469.
(9) Bryan, C. D.; Cordes, A. W.; Haddon, R. C.; Hicks, R. G.; Kennepohl, D. K.; MacKinnon, C. D.; Oakley, R. T.; Palstra, T. T. M.; Perel, A. S.; Scott, S. R.; Schneemeyer, L. F.; Waszczak, J. V. *J. Am. Chem. Soc.* **1994**, *116*, 1205.
(10) Seber, G.; Freitas, R. S.; Mague, J. T.; Paduan-Filho, A.; Gratens, X.; Bindilatti, V.; Oliveira, N. F.; Yoshioka, N.; Lahti, P. M. *J. Am. Chem. Soc.* **2012**, *134*, 3825.
(11) Pal, S. K.; Bag, P.; Itkis, M. E.; Tham, F. S.; Haddon, R. C. *J. Am. Chem. Soc.* **2014**, *136*, 14738.
(12) Mandal, S. K.; Samanta, S.; Itkis, M. E.; Jensen, D. W.; Reed, R. W.; Oakley, R. T.; Tham, F. S.; Donnadieu, B.; Haddon, R. C. *J. Am. Chem. Soc.* **2006**, *128*, 1982.
(13) Sarkar, A.; Pal, S. K.; Itkis, M. E.; Liao, P.; Tham, F. S.; Donnadieu, B.; Haddon, R. C. *Chem. Mater.* **2009**, *21*, 2226.
(14) Sarkar, A.; Itkis, M. E.; Tham, F. S.; Haddon, R. C. *Chem. - Eur. J.* **2011**, *17*, 11576.
(15) Small, D.; Zaitsev, V.; Jung, Y.; Rosokha, S. V.; Head-Gordon, M.; Kochi, J. K. *J. Am. Chem. Soc.* **2004**, *126*, 13850.
(16) Small, D.; Rosokha, S. V.; Kochi, J. K.; Head-Gordon, M. *J. Phys. Chem. A* **2005**, *109*, 11261.
(17) Suzuki, S.; Morita, Y.; Fukui, K.; Sato, K.; Shiomi, D.; Takui, T.; Nakasuji, K. *J. Am. Chem. Soc.* **2006**, *128*, 2530.
(18) Mota, F.; Miller, J. S.; Novoa, J. J. *J. Am. Chem. Soc.* **2009**, *131*, 7699.
(19) Cui, Z.; Lischka, H.; Beneberu, H. Z.; Kertesz, M. *J. Am. Chem. Soc.* **2014**, *136*, 5539.
(20) Morita, Y.; Suzuki, S.; Sato, K.; Takui, T. *Nat. Chem.* **2011**, *3*, 197.
(21) Niyogi, S.; Bekyarova, E.; Hong, J.; Khizroev, S.; Berger, C.; de Heer, W. A.; Haddon, R. C. *J. Phys. Chem. Lett.* **2011**, *2*, 2487.
(22) Goto, K.; Kubo, T.; Yamamoto, K.; Nakasuji, K.; Sato, K.; Shiomi, D.; Takui, T.; Kubota, M.; Kobayashi, T.; Yakusi, K.; Ouyang, J. *J. Am. Chem. Soc.* **1999**, *121*, 1619.
(23) Koutentis, P. A.; Chen, Y.; Cao, Y.; Best, T. P.; Itkis, M. E.; Beer, L.; Oakley, R. T.; Brock, C. P.; Haddon, R. C. *J. Am. Chem. Soc.* **2001**, *123*, 3864.
(24) Beer, L.; Mandal, S. K.; Reed, R. W.; Oakley, R. T.; Tham, F. S.; Donnadieu, B.; Haddon, R. C. *Cryst. Growth Des.* **2007**, *7*, 802.
(25) Mou, Z.; Uchida, K.; Kubo, T.; Kertesz, M. *J. Am. Chem. Soc.* **2014**, *136*, 18009.
(26) Tian, Y.-H.; Sumpter, B. G.; Du, S.; Huang, J. *J. Phys. Chem. Lett.* **2015**, *6*, 2318.
(27) Pal, S. K.; Itkis, M. E.; Tham, F. S.; Reed, R. W.; Oakley, R. T.; Haddon, R. C. *Science* **2005**, *309*, 281.
(28) Anderson, P. W. *Mater. Res. Bull.* **1973**, *8*, 153.
(29) Anderson, P. W. *Science* **1987**, *235*, 1196.
(30) Hicks, R. G. *Org. Biomol. Chem.* **2007**, *5*, 1321.
(31) Hicks, R. G. *Nat. Chem.* **2011**, *3*, 189.
(32) Fujita, W.; Awaga, K. *Science* **1999**, *286*, 261.
(33) Morita, Y.; Suzuki, S.; Fukui, K.; Nakazawa, S.; Kitagawa, H.; Kishida, H.; Okamoto, H.; Naito, A.; Sekine, A.; Ohashi, Y.; Shiro, M.; Sasaki, K.; Shiomi, D.; Sato, K.; Takui, T.; Nakasuji, K. *Nat. Mater.* **2008**, *7*, 48.
(34) Robertson, C. M.; Leitch, A. A.; Cvrkalj, K.; Myles, D. J. T.; Reed, R. W.; Dube, P. A.; Oakley, R. T. *J. Am. Chem. Soc.* **2008**, *130*, 14791.
(35) Winter, S. M.; Datta, S.; Hill, S.; Oakley, R. T. *J. Am. Chem. Soc.* **2011**, *133*, 8126.
(36) Shimizu, A.; Uruichi, M.; Yakushi, K.; Matsuzaki, H.; Okamoto, H.; Nakano, M.; Hirao, Y.; Matsumoto, K.; Kurata, H.; Kubo, T. *Angew. Chem., Int. Ed.* **2009**, *48*, 5482.
(37) Herrmann, C.; Solomon, G. C.; Ratner, M. A. *J. Am. Chem. Soc.* **2010**, *132*, 3682.
(38) Pal, S. K.; Bag, P.; Sarkar, A.; Chi, X. L.; Itkis, M. E.; Tham, F. S.; Donnadieu, B.; Haddon, R. C. *J. Am. Chem. Soc.* **2010**, *132*, 17258.
(39) Pariyar, A.; Vijaykumar, G.; Bhunia, M.; Dey, S. K.; Singh, S. K.; Kurungot, S.; Mandal, S. K. *J. Am. Chem. Soc.* **2015**, *137*, 5955.
(40) Wolf, S. A.; Chtchelkanova, A. Y.; Treger, D. M. *IBM J. Res. Dev.* **2006**, *50*, 101.

DOI: 10.1021/jacs.5b06145
J. Am. Chem. Soc. 2015, 137, 10000−10008

(41) Parkin, S. S. P.; Hayashi, M.; Thomas, L. *Science* **2008**, *320*, 190.
(42) Raman, K. V.; Kamerbeek, A. M.; Mukherjee, A.; Atodiresei, N.; Sen, T. K.; Lazic, P.; Caciuc, V.; Michel, R.; Stalke, D.; Mandal, S. K.; Blugel, S.; Munzenberg, M.; Moodera, J. S. *Nature* **2013**, *493*, 509.
(43) Fuchs, G. D.; Burkard, G.; Klimov, P. V.; Awschalom, D. D. *Nat. Phys.* **2011**, *7*, 789.
(44) Pauling, L. *Nature* **1948**, *161*, 1019.
(45) Sze, S. M. *Physics of Semiconductor Devices*; Wiley: New York, 1981.
(46) Haddon, R. C. *Acc. Chem. Res.* **1992**, *25*, 127.
(47) Haddon, R. C.; Chichester, S. V.; Marshall, J. H. *Tetrahedron* **1986**, *42*, 6293.
(48) Haddon, R. C.; Hirani, A. M.; Kroloff, N. J.; Marshall, J. H. *J. Org. Chem.* **1983**, *48*, 2115.
(49) Haddon, R. C.; Rayford, R.; Hirani, A. M. *J. Org. Chem.* **1981**, *46*, 4587.
(50) *APEX 2*, version 2014.1-1; Bruker AXS Inc.: Madison, WI, 2014.
(51) *SADABS*, 2012/1; Bruker AXS Inc.: Madison, WI, 2012.
(52) Cordes, A. W.; Haddon, R. C.; Oakley, R. T.; Schneemeyer, L. F.; Waszczak, J. V.; Young, K. M.; Zimmerman, N. M. *J. Am. Chem. Soc.* **1991**, *113*, 582.
(53) Andrews, M. P.; Cordes, A. W.; Douglass, D. C.; Fleming, R. M.; Glarum, S. H.; Haddon, R. C.; Marsh, P.; Oakley, R. T.; Palstra, T. T. M.; Schneemeyer, L. F.; Trucks, G. W.; Tycko, R.; Waszczak, J. V.; Young, K. M.; Zimmerman, N. M. *J. Am. Chem. Soc.* **1991**, *113*, 3559.
(54) Haddon, R. C.; Siegrist, T.; Fleming, R. M.; Bridenbaugh, P. M.; Laudise, R. A. *J. Mater. Chem.* **1995**, *5*, 1719.
(55) Haddon, R. C.; Chi, X.; Itkis, M. E.; Anthony, J. E.; Eaton, D. L.; Siegrist, T.; Mattheus, C. C.; Palstra, T. T. M. *J. Phys. Chem. B* **2002**, *106*, 8288.

DOI: 10.1021/jacs.5b06145
J. Am. Chem. Soc. 2015, 137, 10000−10008